

Neutral MSSM Higgs-boson production at e^+e^- colliders in the Feynman-diagrammatic approach

S. Heinemeyer^{1,a}, W. Hollik^{2,b}, J. Rosiek^{3,4,c}, G. Weiglein^{5,d}

¹ HET, Physics Department, Brookhaven Natl. Lab., Upton, NY 11973, USA

² Institut für Theoretische Physik, Universität Karlsruhe, 76128 Karlsruhe, Germany

³ Physik-Department, Technische Universität München, 85747 Garching, Germany

⁴ Institute of Theoretical Physics, Warsaw University, 00681 Warsaw, Poland

⁵ CERN, TH Division, 1211 Geneva 23, Switzerland

Received: 7 February 2001 / Published online: 23 March 2001 – © Springer-Verlag 2001

Abstract. We calculate the cross sections for the neutral Higgs-boson production at e^+e^- colliders in the Minimal Supersymmetric Standard Model (MSSM) using the Feynman-diagrammatic approach and the on-shell renormalization scheme. We incorporate the Higgs-boson propagator corrections, evaluated up to two-loop order, into the prediction of the cross sections for the Higgs-boson production mechanism $e^+e^- \rightarrow hZ, hA$. The propagator corrections consist of the full one-loop contribution, including the effects of non-vanishing external momentum, and at the two-loop level of the dominant corrections of $\mathcal{O}(\alpha\alpha_s)$ and further sub-dominant contributions. The results are supplemented with the complete set of one-loop vertex and box corrections. The effects of the two-loop propagator corrections are investigated in detail. We briefly discuss also the effect of the box contributions for high \sqrt{s} . We compare our results with the case where only the corrections to the effective mixing angle, evaluated within the renormalization-group-improved one-loop Effective Potential approach, are taken into account. We find agreement better than 10% for LEP2 energies and deviations larger than 20% for $\sqrt{s} = 500$ GeV.

1 Introduction

The search for the light neutral Higgs boson is a crucial test of Supersymmetry that can be performed with the present and the next generation of accelerators. The prediction of a relatively light Higgs boson is common to all supersymmetric models whose couplings remain in the perturbative regime up to a very high energy scale [1]. Finding the Higgs boson is thus one of the main goals of high-energy physics. Possible indications for a Higgs boson with a mass around 115 GeV have recently been observed in the LEP analysis [2]. As a second step, once a scalar particle has been found, it is necessary to measure the dominant production cross sections as well as the decay widths and branching ratios of the main decay channels to a high accuracy. Such precise measurements of Higgs–gauge-boson and Higgs–Yukawa couplings allow to experimentally investigate the details of the Higgs mechanism. Finally, also the Higgs self-couplings will have to be measured in order to reconstruct the Higgs potential. A future linear e^+e^- collider with high luminosity [3] can provide a sufficiently clean environment to measure both the Higgs

couplings to other particles as well as its self couplings [4] with high precision, allowing to distinguish between a standard and a non-standard Higgs boson. In this paper we concentrate on the production of the neutral Higgs bosons of the Minimal Supersymmetric Standard Model (MSSM) in e^+e^- annihilations and provide results for the production cross sections for general model parameters, together with a detailed numerical study.

In the MSSM, the mass of the lightest Higgs boson, M_h , is bounded from above by $M_h \lesssim 135$ GeV, including radiative corrections up to two-loop order [5–10, 12, 13, 11]. The most promising channels for the production of the supersymmetric neutral Higgs particles at LEP2 energies and in the first phase of future e^+e^- colliders are the Higgs-strahlung process [14]

$$e^+e^- \rightarrow Zh(H), \quad (1)$$

and the associated production of a scalar and a pseudoscalar Higgs boson

$$e^+e^- \rightarrow Ah(H). \quad (2)$$

We compute the MSSM predictions for the cross sections of both channels in the Feynman-diagrammatic (FD) approach using the on-shell renormalization scheme. We take into account the complete set of one-loop contribu-

^a e-mail: Sven.Heinemeyer@bnl.gov

^b e-mail: Wolfgang.Hollik@physik.uni-karlsruhe.de

^c e-mail: Janusz.Rosiek@ph.tum.de

^d e-mail: Georg.Weiglein@cern.ch

tions, thereby keeping the full dependence on all kinematical variables. The one-loop contributions consist of the corrections to the Higgs- and gauge-boson propagators, where the former contain the dominant electroweak one-loop corrections of $\mathcal{O}(G_F m_t^4)$, and of the contributions to the 3-point and 4-point vertex functions [15–19]. We combine the complete one-loop result with the dominant two-loop QCD corrections of $\mathcal{O}(G_F \alpha_s m_t^4)$ [12, 13] and further sub-dominant corrections. In this way the currently most accurate results for the cross sections are obtained.

Furthermore we show analytically that the Higgs-boson propagator corrections with neglected momentum dependence can be absorbed into the tree-level coupling using the effective mixing angle from the neutral \mathcal{CP} -even Higgs-boson sector. We compare our results for the cross sections with the approximation in which only the corrections to the effective mixing angle, evaluated within the renormalization-group-improved one-loop Effective Potential approach, are taken into account. For most parts of the MSSM parameter space we find agreement better than 10% for the highest LEP energies, while for $\sqrt{s} = 500$ GeV the difference can reach 25%.

The paper is organized as follows: in Sect. 2 the basic formulae are presented and it is shown analytically how the Higgs-boson-propagator corrections with neglected external momenta are related to the effective mixing angle in the Effective Potential approach (EPA). Section 3 contains the numerical analysis for the production cross sections and the comparison of our full result with the EPA. The conclusions can be found in Sect. 4.

2 Cross sections for Higgs-particle production in e^+e^- collisions

2.1 Classification of radiative corrections

The two Higgs-field doublets giving rise to electroweak symmetry breaking within the MSSM accommodate five physical Higgs bosons [20]. At the tree-level, two input parameters (besides the parameters of the Standard Model (SM) gauge-sector) are needed to describe the Higgs sector. We choose them to be $\tan\beta$, the ratio of the two vacuum expectation values, and M_A , the mass of the \mathcal{CP} -odd Higgs boson. The \mathcal{CP} -even neutral mass eigenstates are obtained from the interaction eigenstates by the rotation

$$\begin{pmatrix} H_1 \\ H_2 \end{pmatrix} \equiv \begin{pmatrix} H \\ h \end{pmatrix} = \begin{pmatrix} \cos\alpha & \sin\alpha \\ -\sin\alpha & \cos\alpha \end{pmatrix} \begin{pmatrix} \phi_1^0 \\ \phi_2^0 \end{pmatrix} \quad (3)$$

with the tree-level mixing angle α related to $\tan\beta$, M_A and M_Z by

$$\tan 2\alpha = \tan 2\beta \frac{M_A^2 + M_Z^2}{M_A^2 - M_Z^2}, \quad -\frac{\pi}{2} < \alpha < 0. \quad (4)$$

Two main sources for the production of supersymmetric Higgs particles in e^+e^- collisions are the Higgs-strahlung process [14]

$$e^+e^- \rightarrow ZH_i, \quad i = 1, 2 \quad (5)$$

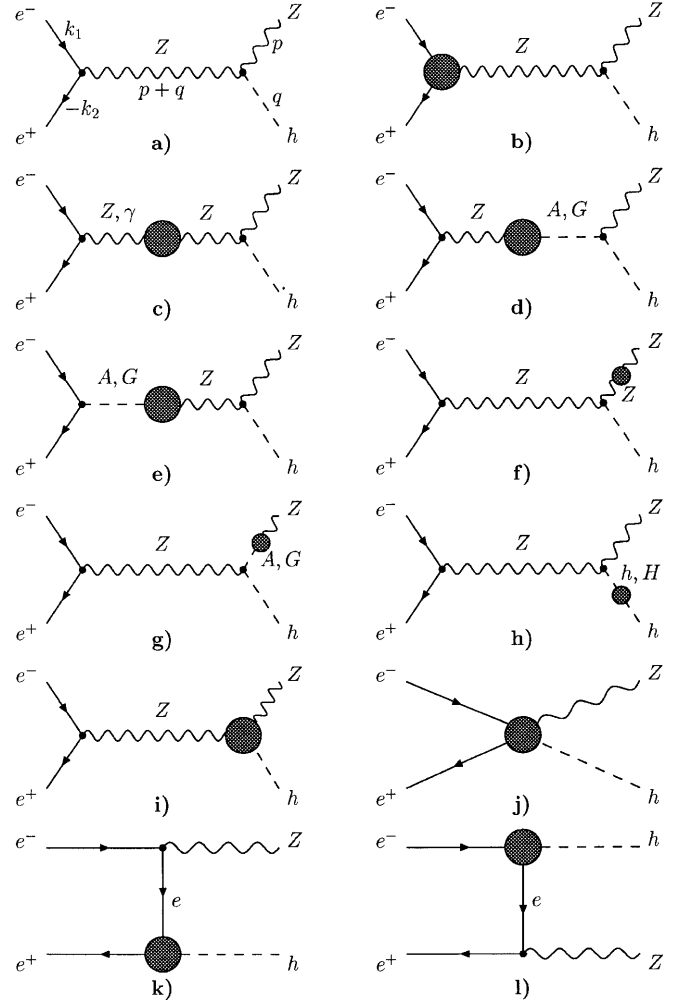


Fig. 1. Generic diagrams contributing to the $e^+e^- \rightarrow Zh$ cross section

(using the compact notation of (3)) and the associated production of scalar and pseudoscalar Higgs bosons,

$$e^+e^- \rightarrow AH_i, \quad i = 1, 2. \quad (6)$$

We do not discuss here the possibility of Higgs-particle production by bremsstrahlung off heavy quarks (e.g. $e^+e^- \rightarrow \bar{b}bH_i$, which can be significant for large $\tan\beta$ [21]), or by W^+W^- fusion, which becomes important for center of mass system (CMS) energies of $\mathcal{O}(500$ GeV) [14].

The set of diagrams taken into account for Higgs-strahlung $e^+e^- \rightarrow hZ$ is schematically shown in Fig. 1, where a) is the tree-level diagram. The shaded blobs summarize the loops with all possible virtual particles, except photons in the Ze^+e^- vertex corrections¹. More details can be found in [16, 18, 19]. An analogous set has been evaluated for the second process, $e^+e^- \rightarrow hA$.

For completeness, in Fig. 1 also contributions are shown (e.g. the A, G - Z mixing contributions and the lon-

¹ These virtual IR-divergent photonic corrections constitute, together with real-photon bremsstrahlung, the initial-state QED corrections, which are conventionally treated separately and are the same as for the SM Higgs-boson production

gitudinal parts of the Z and γ - Z self-energies) that are proportional to the electron mass or vanish completely after contraction with the polarization vector of the Z boson. The different types of corrections can be summarized as follows:

- (i) Corrections to the e , Z , γ and γ - Z self-energies on the internal and external lines and to the (initial state) Ze^+e^- and γe^+e^- vertices, b) – g).
- (ii) Corrections to the scalar and pseudoscalar propagators, h).
- (iii) Corrections to the ZZH_i (ZAH_i) vertex, i).
- (iv) Box-diagram contributions and t -channel-exchange diagrams, j) – l).

The corrections (i)-(iv) have a different relative impact:

- Electroweak corrections of type (i) are typically of the order of a few percent (like in the Standard Model) and do not exhibit a strong dependence on any SUSY parameters.
- The main source of differences between the tree-level and higher-order results are the corrections to the Higgs-boson self-energies (ii). They are responsible for changes in the physical masses M_h and M_H and the effective mixing angle α_{eff} (via contributions to the renormalization constants, \mathcal{Z}^{ext} , for the external Higgs particles in the S -matrix elements, see Sect. 2.2) predicted for given values of $\tan\beta$ and M_A . At the one-loop level these propagator corrections constitute the only source for the large correction of $\mathcal{O}(G_F m_t^4)$. At the two-loop level they exclusively give rise to contributions of $\mathcal{O}(G_F \alpha_s m_t^4)$ and of $\mathcal{O}(G_F^2 m_t^6)$. In this sense the propagator corrections define a closed subset of diagrams, being responsible for a numerically large contribution.
- Corrections to the final-state vertices (iii) are typically larger than those of type (i), but smaller than the Higgs-boson propagator corrections. At LEP2 energies they can reach at most 7-10% [16] for very low or very large values of $\tan\beta$, when the Yukawa couplings of the top or bottom quarks become strong.
- Finally, the box-diagram contributions (iv) depend strongly on the center-of-mass energy. They are of the order of 2-3% at LEP2 energies and may reach 20% for $\sqrt{s} = 500$ GeV [19].

It should be noted that initial-state QED corrections as well as finite-width effects (allowing for off-shell decays of the Higgs and the Z boson) are not included in our calculation. However, by incorporating our result into existing codes, e.g. HZHA [22], QED corrections and finite-width effects can automatically be taken into account².

2.2 Higgs-boson masses and wave function renormalizations

Radiative corrections induce mixing between the \mathcal{CP} -even Higgs bosons, even if their mass matrix has been diagonalized at the tree level³. In the FD approach the higher-order corrected Higgs-boson masses, denoted by M_h, M_H , are derived by finding the poles of the h, H -propagator matrix, which is given by

$$\hat{\mathbf{D}}_S = \begin{pmatrix} \Delta_H & \Delta_{hH} \\ \Delta_{hH} & \Delta_h \end{pmatrix} \quad (7)$$

$$= i \begin{pmatrix} q^2 - m_H^2 + \hat{\Sigma}_{HH}(q^2) & \hat{\Sigma}_{hH}(q^2) \\ \hat{\Sigma}_{hH}(q^2) & q^2 - m_h^2 + \hat{\Sigma}_{hh}(q^2) \end{pmatrix}^{-1}.$$

Here the $\hat{\Sigma}(q^2)$ denote the renormalized Higgs-boson self-energies (throughout the paper we denote tree-level mass parameters by small letters and physical masses by capital letters). For these self-energies we take the result of the complete one-loop on-shell calculation of [15, 16] together with the dominant two-loop correction of $\mathcal{O}(\alpha\alpha_s)$ obtained in [12, 13] and the sub-dominant corrections of $\mathcal{O}(G_F^2 m_t^6)$ [6–8].

Determining the poles of (7) corresponds to solving the equation

$$\text{Re} \left[\left(q^2 - m_h^2 + \hat{\Sigma}_{hh}(q^2) \right) \left(q^2 - m_H^2 + \hat{\Sigma}_{HH}(q^2) \right) - \left(\hat{\Sigma}_{hH}(q^2) \right)^2 \right] = 0. \quad (8)$$

The wave function renormalization factors for the scalar Higgs bosons H_i are denoted as $\mathcal{Z}_{S_i}^{\text{ext}}$. They are the finite residues of the H and h propagators, respectively,

$$\mathcal{Z}_{S_1}^{\text{ext}} \equiv \mathcal{Z}_{S_H}^{\text{ext}} = \left(1 + \text{Re} \hat{\Sigma}'_{HH}(q^2) - \text{Re} \left(\frac{\hat{\Sigma}_{hH}^2(q^2)}{q^2 - m_h^2 + \hat{\Sigma}_{hh}(q^2)} \right)' \right)^{-1} \Bigg|_{q^2=M_H^2},$$

$$\mathcal{Z}_{S_2}^{\text{ext}} \equiv \mathcal{Z}_{S_h}^{\text{ext}} = \left(1 + \text{Re} \hat{\Sigma}'_{hh}(q^2) - \text{Re} \left(\frac{\hat{\Sigma}_{hH}^2(q^2)}{q^2 - m_H^2 + \hat{\Sigma}_{HH}(q^2)} \right)' \right)^{-1} \Bigg|_{q^2=M_h^2}, \quad (9)$$

where $\hat{\Sigma}'(q^2) \equiv \frac{\partial}{\partial q^2} \hat{\Sigma}(q^2)$.

For a diagram with no mixing on the outgoing Higgs-boson line, H_i , the S -matrix element is given by the amputated on-shell Green's function multiplied by the $(\mathcal{Z}_{S_i}^{\text{ext}})^{1/2}$. In the presence of mixing, i.e. $h \leftrightarrow H$ on the external line (with the scalar i being the final state particle) the respective factor reads:

$$\left\{ \left(-\hat{\Sigma}_{hH}(q^2) (\mathcal{Z}_{S_i}^{\text{ext}})^{-1/2} (q^2 - M_{H_i}^2) \right) \right\} /$$

² The implementation of our calculation into HZHA is currently investigated [23]

³ We do not consider here possible \mathcal{CP} -violating mixing between neutral Higgs bosons, which can occur if the MSSM Lagrangian contains complex parameters [24]

$$\left(\left(q^2 - m_H^2 + \hat{\Sigma}_{HH}(q^2) \right) \left(q^2 - m_h^2 + \hat{\Sigma}_{hh}(q^2) \right) - \left(\hat{\Sigma}_{hH}(q^2) \right)^2 \right) \Big|_{q^2=M_{H_i}^2} \quad (10)$$

Therefore, in this case, the amputated Green's function is effectively multiplied by (i' denotes the index of the ‘‘supplementary’’ Higgs boson: $i' = 2(1)$ for $i = 1(2)$); formally $i' = 3 - i$)

$$\left(\mathcal{Z}_{S_i}^{\text{ext}} \right)^{1/2} \frac{-\hat{\Sigma}_{hH}(M_{H_i}^2)}{M_{H_i}^2 - m_{H_{i'}}^2 + \hat{\Sigma}_{i'i'}(M_{H_i}^2)} \equiv \left(\mathcal{Z}_{S_i}^{\text{ext}} \right)^{1/2} \mathcal{Z}_{S_i}^{\text{mix}} \quad (11)$$

Exactly analogous equations hold for the pseudoscalar constants $\mathcal{Z}_{P_i}^{\text{ext}}$ and $\mathcal{Z}_{P_i}^{\text{mix}}$. Their effects, however, are numerically much less important. Appropriate formulae for the inclusion of the \mathcal{Z} factors into the higher-order corrected vertices can be found in the Appendix.

2.3 The α_{eff} approximation

The inclusion of the \mathcal{Z} factors on the external Higgs lines in the on-shell calculation reproduces, in the approximation of the neglected momentum dependence of the Higgs self-energies, the effect of using the higher-order corrected angle α_{eff} in an improved Born approximation of the cross sections (see also [25]).

The dominant contributions for the Higgs-boson self-energies (of $\mathcal{O}(G_F m_t^4)$ at the one-loop level) are obtained for $q^2 = 0$. Approximating the renormalized Higgs-boson self-energies by

$$\hat{\Sigma}(q^2) \rightarrow \hat{\Sigma}(0) \equiv \hat{\Sigma} \quad (12)$$

yields the Higgs-boson masses by re-diagonalizing the dressed mass matrix

$$\hat{M}_{\text{Higgs}}^2 = \begin{pmatrix} m_H^2 - \hat{\Sigma}_{HH} & -\hat{\Sigma}_{hH} \\ -\hat{\Sigma}_{hH} & m_h^2 - \hat{\Sigma}_{hh} \end{pmatrix} \xrightarrow{\Delta\alpha} \begin{pmatrix} M_H^2 & 0 \\ 0 & M_h^2 \end{pmatrix}, \quad (13)$$

where M_h and M_H are the corresponding higher-order-corrected Higgs-boson masses. In [25] it has been shown that in the approximation with neglected external momentum the \mathcal{Z}^{mix} factors can be written as follows in terms of $\Delta\alpha$, which is the angle required for the re-diagonalization in (13):

$$\mathcal{Z}_{S_1}^{\text{mix}} \equiv \mathcal{Z}_{S_H}^{\text{mix}} \stackrel{q^2=0}{\approx} -\frac{\hat{\Sigma}_{hH}}{M_H^2 - m_h^2 + \hat{\Sigma}_{hh}} = +\tan \Delta\alpha, \quad (14)$$

$$\mathcal{Z}_{S_2}^{\text{mix}} \equiv \mathcal{Z}_{S_h}^{\text{mix}} \stackrel{q^2=0}{\approx} -\frac{\hat{\Sigma}_{hH}}{M_h^2 - m_H^2 + \hat{\Sigma}_{HH}} = -\tan \Delta\alpha. \quad (15)$$

It is important to note that, although it is not immediately visible, both (14,15) yield the same angle $\Delta\alpha$ [25]:

$$\Delta\alpha = \arctan \frac{\Delta m^2 + \sqrt{(\Delta m^2)^2 + 4 \hat{\Sigma}_{hH}^2}}{-2 \hat{\Sigma}_{hH}}, \quad (16)$$

where

$$\Delta m^2 \equiv (m_H^2 - \hat{\Sigma}_{HH}) - (m_h^2 - \hat{\Sigma}_{hh}). \quad (17)$$

The \mathcal{Z}^{ext} factor can be expressed as

$$\mathcal{Z}_{S_1}^{\text{ext}} \stackrel{q^2=0}{\approx} \mathcal{Z}_{S_2}^{\text{ext}} \stackrel{q^2=0}{\approx} \frac{1}{1 + \tan^2 \Delta\alpha} = \cos^2 \Delta\alpha. \quad (18)$$

The consequences for the couplings are demonstrated for Zh production in the following example for the ZZh vertex. The Born coupling $\tilde{V}_{ZZh} \sim -\sin(\alpha - \beta)$ is changed by the loop corrections, in terms of the \mathcal{Z} factors, according to

$$\begin{aligned} \tilde{V}_{ZZh} &\sim \left(\mathcal{Z}_{S_h}^{\text{ext}} \right)^{\frac{1}{2}} \left[-\sin(\alpha - \beta) - \mathcal{Z}_{S_h}^{\text{mix}} \cos(\alpha - \beta) \right] \\ &= \cos \Delta\alpha \left[-\sin(\alpha - \beta) - (-\tan \Delta\alpha) \cos(\alpha - \beta) \right] \\ &= -\sin(\alpha - \beta + \Delta\alpha) \\ &= -\sin(\alpha_{\text{eff}} - \beta). \end{aligned} \quad (19)$$

Analogous results hold for all Higgs vertices, including the AH_i vertices. Therefore, the \mathcal{Z} factors effectively shift the tree-level angle α by $\Delta\alpha$, yielding a loop-improved angle

$$\alpha_{\text{eff}} = \alpha + \Delta\alpha \quad (20)$$

in this approximation.

While the α_{eff} approximation, i.e. using an improved Born result for the cross sections where the tree-level angle α is replaced by α_{eff} , incorporates the dominant one-loop and two-loop contributions, it is obvious from the discussion above that this approximation neglects many effects included in a full FD calculation. These are contributions from the full spectrum of the MSSM particles, the momentum dependence of the Higgs-boson self-energies, the gauge-boson and the fermion self-energy corrections, and in particular the process-specific vertex and box corrections.

2.4 Cross sections

In this section analytical formulae are presented for the cross sections for the on-shell production of the Higgs bosons $e^+e^- \rightarrow ZH_i$, $e^+e^- \rightarrow AH_i$ including the corrections (i)-(iii). Box diagrams (iv) give another, more complicated, set of formfactors that make the expressions quite lengthy and are hence omitted here; more details can be found in [18]. However, we include the box-diagram contributions, as described in [19], in our numerical programs [26] and in the figures presented in this paper.

The presented formalism for cross sections is general enough to accommodate corrections of any order to 2- and 3-point vertex functions. Beyond the one-loop level, however, currently only two-loop corrections to the scalar propagators have been calculated [12,13]. Therefore, in the cross section calculations we include all possible types of one-loop corrections and the available two-loop corrections to scalar self-energies. This is well justified because, as discussed above, propagator corrections constitute a

closed subset of the leading $\mathcal{O}(G_F\alpha_s m_t^4)$ and $\mathcal{O}(G_F^2 m_t^6)$ contributions. Therefore, these two-loop corrections are of particular relevance and interest.

The cross sections (in the CMS) for both processes (5) and (6) have the form:

$$\frac{d\sigma_{Z(A)H_i}}{d\Omega} = \frac{\lambda(s, M_{Z(A)}^2, M_{H_i}^2)}{64\pi^2 s^2 |D_Z(s)|^2} \times (\mathcal{A}_1 + \mathcal{A}_2 \cos^2 \theta_{\text{CMS}}), \quad (21)$$

where λ is the standard phase space factor,

$$\lambda(s, m_1^2, m_2^2) = \sqrt{s^2 + m_1^4 + m_2^4 - 2sm_1^2 - 2sm_2^2 - 2m_1^2 m_2^2}, \quad (22)$$

and $\mathcal{A}_1, \mathcal{A}_2$ are defined by

$$\mathcal{A}_1 + \mathcal{A}_2 \cos^2 \theta_{\text{CMS}} = \frac{1}{4} \sum_{\text{pol}} (\mathcal{M} \mathcal{M}^*), \quad (23)$$

with \mathcal{M}_{ZS} and \mathcal{M}_{PS} as given below. In the following, θ_{CMS} denotes the scattering angle $\theta_{\text{CMS}} = \angle(e^-, H_i)$ in the CMS. The momenta of the incoming electron and positron are denoted as k_1 and k_2 , respectively. The momentum of the outgoing h, H is labeled with q , whereas the outgoing Z, A momentum is denoted as p , see Fig. 1a. The matrix elements for the Higgs-strahlung process and the associated Higgs production read (in the approximation of neglected box diagrams)

$$\mathcal{M}_{ZS}^i = e\bar{v}(k_2)\gamma^\nu \left[\tilde{V}_{ZZS}^{\mu\nu i} (\hat{c}_V - \hat{c}_A \gamma^5) + \tilde{V}_{\gamma ZS}^{\mu\nu i} \frac{D_Z(s)}{D_\gamma(s)} - \tilde{V}_{ZZS}^{(0)\mu\nu i} \frac{\hat{\Sigma}_{\gamma Z}^T(s)}{D_\gamma(s)} \right] u(k_1) \epsilon_\mu(p), \quad (24)$$

$$\mathcal{M}_{PS}^i = e\bar{v}(k_2)\gamma_\mu \left[\tilde{V}_{ZPS}^{\mu ij} (\hat{c}_V - \hat{c}_A \gamma^5) + \tilde{V}_{\gamma PS}^{\mu ij} \frac{D_Z(s)}{D_\gamma(s)} - \tilde{V}_{ZPS}^{(0)\mu ij} \frac{\hat{\Sigma}_{\gamma Z}^T(s)}{D_\gamma(s)} \right] u(k_1). \quad (25)$$

For the corresponding expressions for the box contributions see [18].

In the above expressions $u(k_1)$ and $v(k_2)$ are spinors of the incoming electron-positron pair, $\epsilon_\mu(p)$ is the polarization vector of the outgoing Z . \hat{c}_V, \hat{c}_A are the renormalized vector and axial couplings of the Z boson to an electron-positron pair, at the one-loop level $\hat{c}_A = -1/4s_W c_W + \hat{c}_A^{(1)}$, $\hat{c}_V = (-1 + 4s_W^2)/4s_W c_W + \hat{c}_V^{(1)}$, $c_W^2 \equiv 1 - s_W^2 \equiv M_W^2/M_Z^2$. $\hat{\Sigma}_Z^T(s)$, $\hat{\Sigma}_\gamma(s)$ and $\hat{\Sigma}_{\gamma Z}^T(s)$ denote the renormalized photon and transverse Z boson self-energies. $D_Z(s)$ and $D_\gamma(s)$ are the inverse Z and photon propagators defined as

$$\begin{aligned} D_Z(s) &= s - M_Z^2 + \hat{\Sigma}_Z^T(s), \\ D_\gamma(s) &= s + \hat{\Sigma}_\gamma(s). \end{aligned} \quad (26)$$

Table 1. Quark masses and SUSY parameters (in GeV) used in the numerical analysis

m_t	m_b	$M_{\tilde{q}}$	$M_{\tilde{l}}$	μ	M_2	M_1	M_3
174.3	4.5	1000	300	200	200	$\frac{5}{3}s_W^2/c_W^2 M_2$	$\frac{\alpha_s}{\alpha_{\text{em}}} s_W^2 M_2$

Finally, \tilde{V} denotes the effective neutral Higgs–gauge–boson vertices with the one-loop form factors. The explicit expression for those vertices and for the matrix elements for Higgs-strahlung and associated Higgs production can be found in the Appendix and in [16].

3 Numerical results

3.1 Parameter choice

In the following we present numerical examples for the dependence of the neutral Higgs-boson couplings and cross sections on $\tan\beta$, M_h , and the mixing in the scalar top sector. In all plots, as a typical example, the set of parameters listed in Table 1 has been used, if not stated differently.

m_t and m_b in Table 1 are the quark pole masses. $M_{\tilde{q},\tilde{l}}$ denote the soft SUSY-breaking parameters in the scalar quark and lepton sector, respectively (in the following we also use the notation $M_{SUSY} \equiv M_{\tilde{q}}$) and $M_3 \equiv m_{\tilde{g}}$ denotes the gluino mass. The mixing in the scalar top sector, which plays a prominent role in the physics of the MSSM Higgs sector, is controlled by the off-diagonal term in the scalar-top mass matrix, $m_t X_t \equiv m_t (A_t - \mu \cot\beta)$, in the convention of [13]. In our analysis we have focused on two different values of X_t leading to two extreme values of the physical Higgs-boson mass M_h , as suggested by [13, 27–29]. The lightest MSSM Higgs-boson mass as a function of X_t/M_{SUSY} has a minimum at $X_t/M_{SUSY} \approx 0$, denoted in the following as “no mixing” case. A maximum value is reached at $X_t/M_{SUSY} \approx 2$, denoted further as “maximal mixing”. For the sbottom sector we assume a universal trilinear coupling, $A_b = A_t$. These values and the parameters in Table 1 are understood to be input parameters for the diagrammatic calculation in the on-shell renormalization scheme.

Below we will also perform comparisons with results obtained in the framework of the RG improved one-loop EPA, where the input parameters are understood as $\overline{\text{MS}}$ quantities. To ensure consistency, in the latter case we have transformed the on-shell SUSY input parameters into the corresponding $\overline{\text{MS}}$ values as discussed in [30]. The results shown below for the higher-order corrected Higgs-boson masses and the mixing angle within the RG improved one-loop EPA have been obtained with the Fortran program *subhpole* (based on [6, 7, 30]).

3.2 2-loop corrections to masses and effective couplings

The dependence of the physical neutral Higgs-boson masses on the MSSM parameters at the 2-loop level has

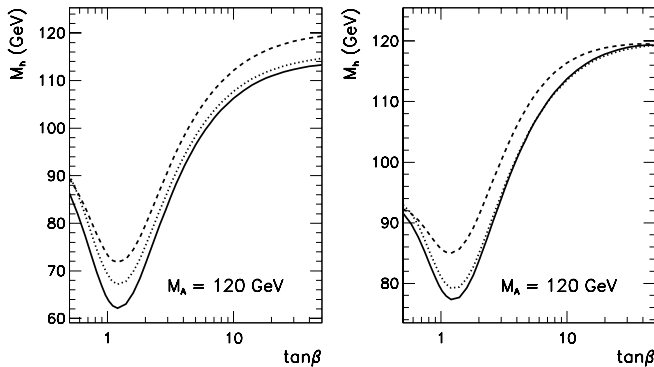


Fig. 2. M_h as a function of $\tan\beta$ for $M_A = 120$ GeV and the parameters of Table 1. The no-mixing (maximal-mixing) case is shown in the left (right) plot. The solid line represents the two-loop FD result, the dotted line shows the RG improved one-loop EPA result and the dashed line shows the one-loop FD result

been extensively discussed in the literature [6–13, 27]. As an illustration, we present in Fig. 2 the dependence of M_h on $\tan\beta$ for a relatively low M_A value, $M_A = 120$ GeV. The two-loop FD result is compared with the RG improved one-loop EPA and also with the one-loop FD result in the no-mixing and in the maximal-mixing scenario in the left and in the right plot of Fig. 2, respectively. In both scenarios M_h shows a similar behavior: a minimum is reached around $\tan\beta \approx 1$, maximum values are reached for the largest $\tan\beta$ values⁴. In the no-mixing scenario the FD result is always smaller than the RG improved one-loop EPA value for M_h , with a maximum difference around $\tan\beta = 1$ of up to 5 GeV. In the maximal-mixing scenario both result mostly agree. Note, however, that this behavior changes for larger values of M_A , where the maximum value of M_h obtained in the FD approach is a few GeV larger than the corresponding RG improved one-loop EPA value [13, 27, 30].

Approximate results for the cross sections have often been obtained in the literature on the basis of improved Born results, where the effective mixing angle α_{eff} , see (20), and the higher-order corrected Higgs-boson masses M_h and M_H have been evaluated within the RG improved one-loop EPA. We will in the following compare our FD result for the cross sections with this approximation, to which we will refer as “RG α_{eff} approximation”. As mentioned above, the results in the RG α_{eff} approximation have been obtained using the program *subhpole* (based on [6, 7, 30]).

In order to disentangle the effect of different contributions in this comparison, we first discuss the results for the effective Z -Higgs-boson couplings in the two approaches. In Sect. 2.3 we have shown that the contribution of the wave function renormalization factors of the Higgs bosons is given by the effective mixing angle α_{eff} evaluated in the FD approach, if the momentum dependence of the Higgs-

boson self-energies is neglected. However, in the actual cross-section calculation in the FD approach the momentum dependence is included at the available (currently one-loop) level. Therefore, for a better comparison of the quantities actually entering the cross section calculation in the two approaches, we formally define α_{eff} in the FD approach as (in analogy to (15))

$$\alpha_{\text{eff}}^h = -\arctan Z_{S^h}^{\text{mix}}, \quad (27)$$

where the $Z_{S^h}^{\text{mix}}$ is given by the exact expression (11) (with Higgs self-energies calculated at $q^2 = M_h^2$), not by the $q^2 = 0$ approximation of (15)⁵.

Using this definition, in Fig. 3 the dependence of $\sin(\alpha_{\text{eff}} - \beta)$ on $\tan\beta$ and M_h is shown in both approaches, for $M_A = 100, 120, 150$ GeV and the no-mixing scenario, $X_t = 0$. Since M_h is a derived quantity and not an input parameter in our approach, the parameter that is actually varied in the plots shown as function of M_h is $\tan\beta$. For simplicity, i.e. in order to avoid a non-functional behavior, in all plots shown as function of M_h in this paper we restrict the $\tan\beta$ region to $\tan\beta > 1.6$ (as mentioned above, for $m_t = 174.3$ GeV and $M_{SUSY} \lesssim 1$ TeV $\tan\beta$ values around 1 are already excluded [31, 28] via Higgs-boson searches.)

As can be seen in Fig. 3, the agreement between the FD two-loop result for α_{eff}^h and the result within the RG improved one-loop EPA is in general remarkably good (while large deviations can appear compared to the FD one-loop result, see e.g. the middle plots in Fig. 3). For most of the $\tan\beta$ range the FD two-loop result and the result within the RG improved one-loop EPA differ by not more than 5%, larger deviations can be observed only for $M_A = 100$ GeV and $\tan\beta > 10$ (left upper plot in Fig. 3), where $\sin(\alpha_{\text{eff}} - \beta)$ itself is small. Even in this case the $\sin(\alpha_{\text{eff}} - \beta)$ values in both approaches agree very well with each other when expressed in terms of the physical Higgs mass M_h . For the maximal-mixing case, $X_t/M_{SUSY} = 2$, the differences between the effective couplings obtained in both methods are even smaller.

It should be noted that the behavior of $\sin(\alpha_{\text{eff}} - \beta)$ in the limit of large $\tan\beta$ is quite different for small and large pseudoscalar masses. This behavior changes for M_A between 100 and 150 GeV; the actual value depends on the stop mixing parameter X_t (see also Fig. 9 in [25].)

3.3 Results for the cross sections

Differences in the Higgs-production cross sections between our FD result (containing the complete one-loop result and the dominant two-loop corrections) and the RG α_{eff} approximation have a two-fold origin: the different predictions for the values of M_h and α_{eff} , which we compared in the previous section, and the additional contributions contained in the FD result (i.e. the one-loop 3- and 4-point vertex functions and the 2-point contributions that are not contained in α_{eff}).

⁴ One should keep in mind, however, that for fixed $m_t = 174.3$ GeV and $M_{SUSY} \lesssim 1$ TeV $\tan\beta$ around 1 is already excluded [31, 28] via Higgs-boson searches

⁵ It should be noted that α_{eff}^H defined as $\alpha_{\text{eff}}^H = \arctan Z_{S^H}^{\text{mix}}$ slightly differs from α_{eff}^h

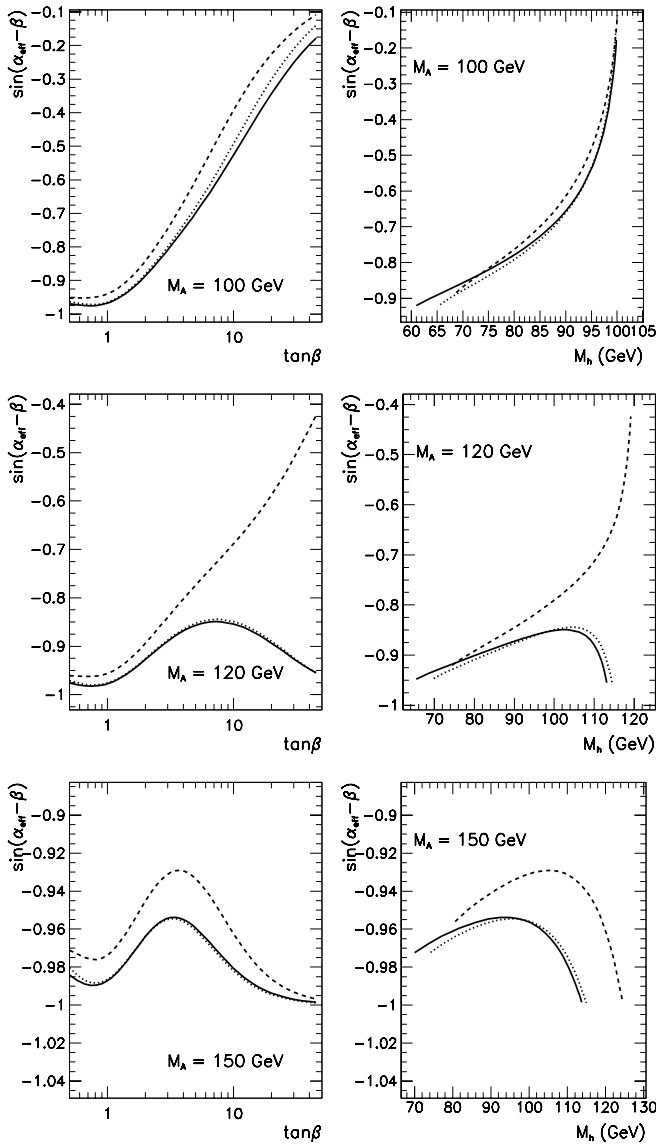


Fig. 3. $\sin(\alpha_{\text{eff}} - \beta)$ as a function of $\tan\beta$ (left plots) and M_h (right plots) for $X_t = 0$ and the parameters of Table 1. The solid line represents the two-loop FD result (see (27)), the dotted line shows the RG improved one-loop EPA result, and the dashed line shows the one-loop FD result

In Fig. 4 we present the cross sections for the two production channels for a LEP2 energy of $\sqrt{s} = 206$ GeV, in the no-mixing and the maximal-mixing scenario, as a function of $\tan\beta$. Fig. 5 shows the same results as a function of M_h . At LEP2 energies, the box diagram contributions are small, of the order of 2-3% [18, 19], and do not modify the cross section behavior in a significant way.

As can be seen from both figures, the cross sections for the Higgs-strahlung process corresponding to the FD result and the RG α_{eff} approximation are close to each other, with differences of the order of a few per cent. The only exception occurs at $X_t \approx 0$ and large $\tan\beta$. In this case the difference can amount up to 50% when the cross sections are expressed as a function of $\tan\beta$, but is con-

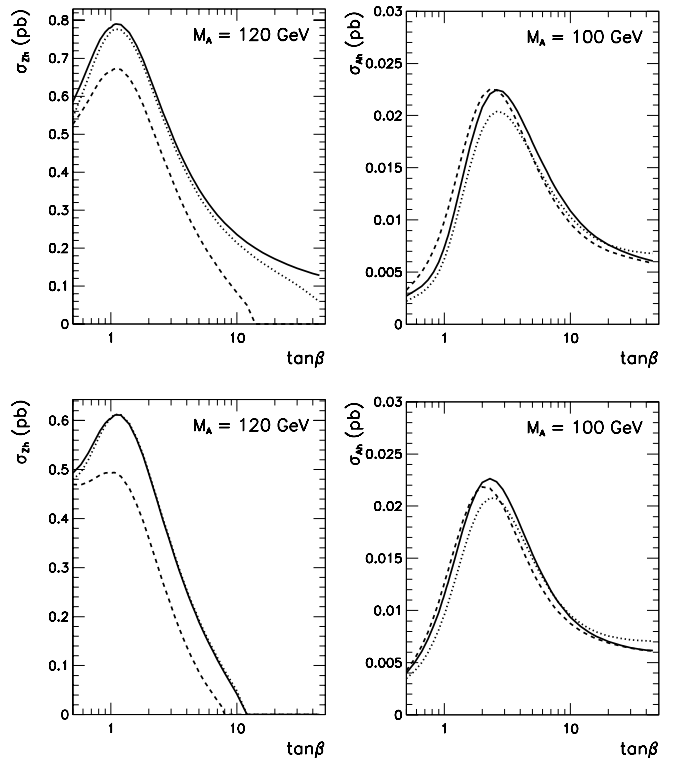


Fig. 4. σ_{Zh} and σ_{Ah} at $\sqrt{s} = 206$ GeV as a function of $\tan\beta$ for two values of M_A and the parameters of Table 1. The upper (lower) row contains the result for the no- (maximal)-mixing scenario. The solid line represents the two-loop FD result, the dotted line shows the result for the RG α_{eff} approximation and the dashed line shows the one-loop FD result

siderably reduced when they are calculated in terms of M_h . The two-loop result in the FD calculation is always above the one-loop result; the difference can be sizable, but is then mostly due to the kinematical effect that the values for M_h at one-loop are much larger than at the two-loop level. This effect is especially pronounced at the kinematical endpoints, i.e. for large $\tan\beta$.

Associated Ah production is of interest at LEP2 energies only for sufficiently low $M_A \leq 120$ GeV, otherwise it is kinematically forbidden. Therefore we restricted our plots for σ_{Ah} in Figs. 4 and 5 to $M_A = 100$ GeV. The difference between the FD result and the RG α_{eff} approximation is larger than for σ_{Zh} and may reach about 20% for not too large $\tan\beta$ values. The result of the two-loop FD calculation is mostly above the one-loop result, but the differences are much smaller than for the Higgs-strahlung process.

For both processes, the differences between the FD result and the RG α_{eff} approximation are not particularly pronounced, however visibly larger than those induced by the modifications of α_{eff} only. For LEP2 energies they can be attributed mostly to the vertex corrections to the ZZh and ZhA couplings [16].

The dependence on the \tilde{t} mixing is depicted in Fig. 6. The main effect on σ_{Zh} , σ_{Ah} is kinematical and arises from the change of M_h with X_t/M_{SUSY} . This effect leads to a

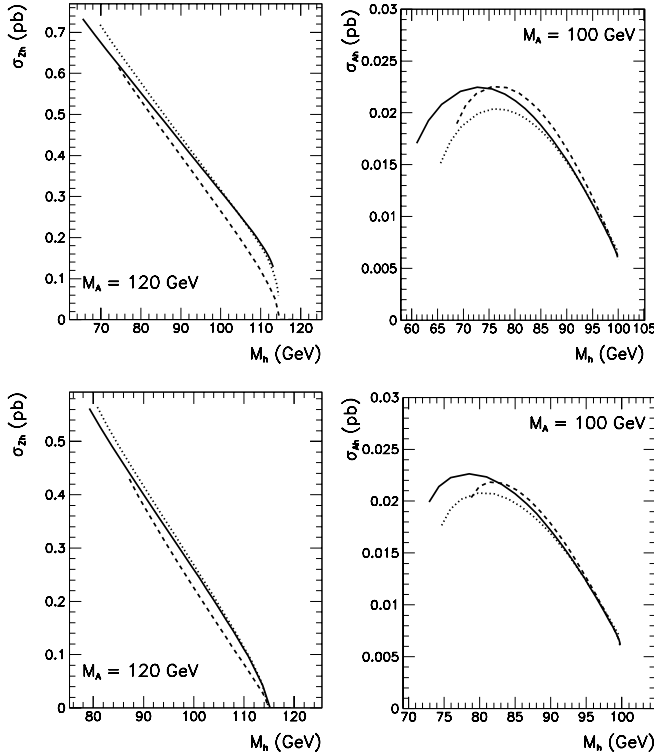


Fig. 5. σ_{Zh} and σ_{Ah} at $\sqrt{s} = 206$ GeV as a function of M_h for two values of M_A and the parameters of Table 1. The upper (lower) row contains the result for the no- (maximal)-mixing scenario. The solid line represents the two-loop FD result, the dotted line shows the result for the RG α_{eff} approximation and the dashed line shows the one-loop FD result

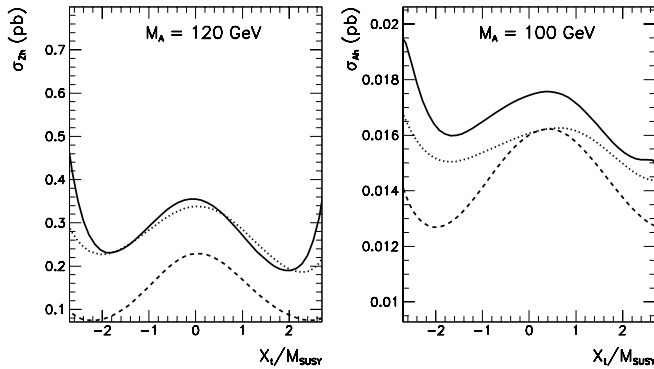


Fig. 6. σ_{Zh} and σ_{Ah} as a function of X_t/M_{SUSY} for $\sqrt{s} = 206$ GeV, $\tan\beta = 5$ and the parameters of Table 1. The solid line represents the two-loop FD result, the dotted line shows the RG α_{eff} approximation and the dashed line shows the one-loop FD result

visible (additional) asymmetry in the two-loop FD results, whereas the RG α_{eff} approximation and the one-loop FD result show a weaker asymmetry in X_t/M_{SUSY} . As can be seen from the figure, the differences between the methods are much larger (typically more than 10%) when associated production is considered, with the above-mentioned

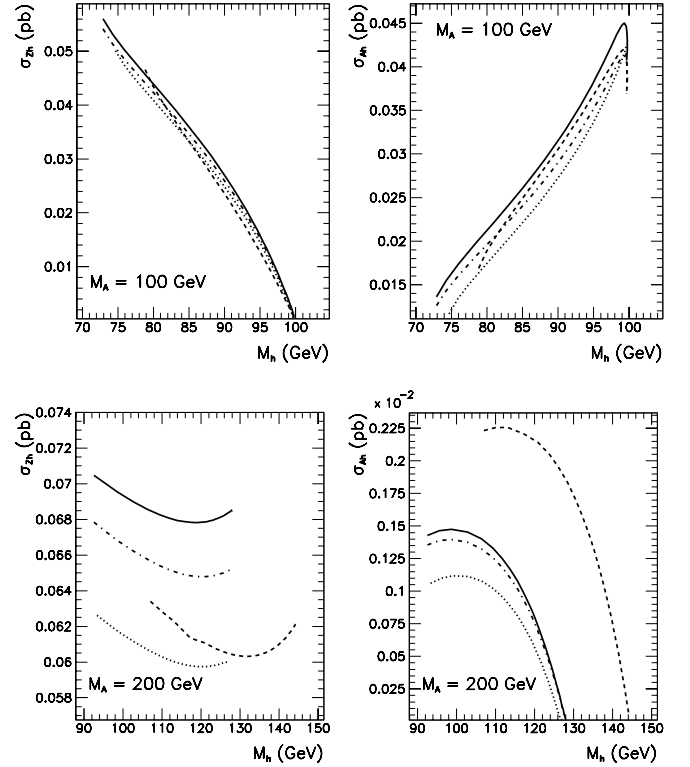


Fig. 7. σ_{Zh} and σ_{Ah} as a function of M_h at $\sqrt{s} = 500$ GeV, for two values of M_A , $X_t/M_{\text{SUSY}} = 2$, and the parameters of Table 1. The solid (dot-dashed) line represents the two-loop FD result including (excluding) box contributions, the dotted line shows the RG α_{eff} approximation and the dashed line shows the one-loop FD result

“kinematical” asymmetry further increased by the inclusion of the vertex corrections.

In Fig. 7 the cross sections for the Higgs-strahlung process and the associated production are shown for a typical Linear Collider energy, $\sqrt{s} = 500$ GeV [3], in the maximal-mixing scenario (in the no-mixing scenario similar results have been obtained). In addition to the previous plots we also show the result for the two-loop FD calculation where the box contributions have not been included, in order to point out their relative importance for high-energy collisions. For $\sqrt{s} = 500$ GeV the differences between the FD result and the RG α_{eff} approximation are larger than in the low-energy scenario, an effect that is more pronounced for the higher value of M_A . For $M_A = 200$ GeV, typically they are of the order of 10-15% for σ_{Zh} and even up to 25% for σ_{Ah} (for $M_h \gtrsim 90$ GeV). The difference between the two-loop and one-loop FD result can be sizable. The two-loop result for σ_{Zh} is in general larger than the one-loop value, again increasing with M_A , where for $M_A = 200$ GeV the difference can amount up to 15%. σ_{Ah} , on the other hand, is decreased at the two-loop level for $M_A = 200$ GeV and the difference may be sizable.

The box contributions become more important for higher \sqrt{s} and change the total cross section by 5-10%. This result remains unchanged even if sleptons are significantly heavier than $M_{\tilde{l}} = 300$ GeV used in our numerical

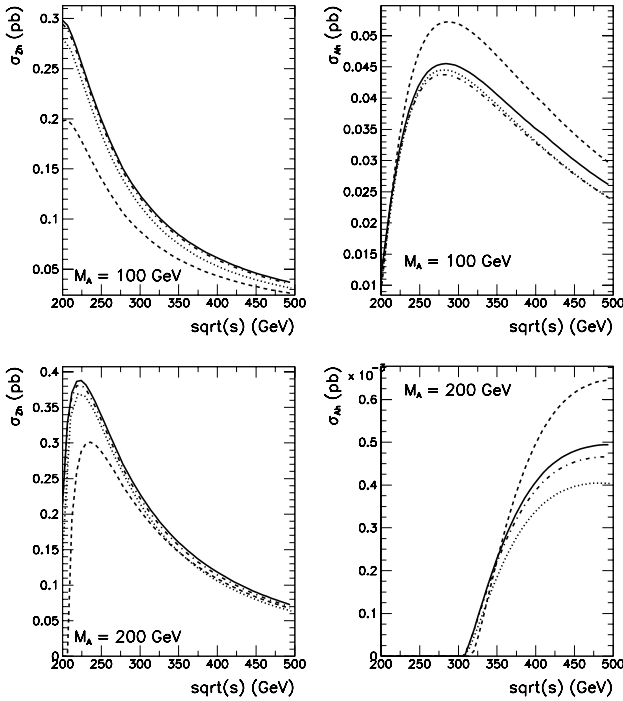


Fig. 8. σ_{Zh} and σ_{Ah} as a function of \sqrt{s} for $\tan\beta = 5$, $X_t = 0$, and the parameters of Table 1. The solid (dot-dashed) line represents the two-loop FD result including (excluding) box contributions, the dotted line shows the RG α_{eff} approximation and the dashed line shows the one-loop FD result

analysis, as the dominant contributions to box diagrams are given by W and Higgs boson exchanges [18, 19], which do not depend on $M_{\tilde{f}}$. Also, one should recall that box contributions lead to an angular distribution of the final-state particles different from the effective Born approximation and thus give much larger corrections to the differential rather than to the total cross section, at least for some range of the scattering angle. Therefore, the box diagrams have a significant effect at Linear Collider energies and thus have to be included. The same conclusions can be drawn for $\sqrt{s} = 500$ GeV in the no-mixing scenario, which we do not show here. The differences between the FD result and the RG α_{eff} approximation are only slightly smaller than in the maximal-mixing case.

In Fig. 8 the results for σ_{Zh} and σ_{Ah} are shown as a function of \sqrt{s} in the no-mixing scenario for $M_A = 100, 200$ GeV. Besides the obvious kinematical drop-off of the cross sections, one can observe that the relative differences between the FD two-loop result and the RG α_{eff} approximation grow with \sqrt{s} . The differences remain almost constant or even increase slowly in absolute terms, whereas the full cross sections decrease. σ_{Ah} becomes very small for large M_A , as can be seen in more detail in Fig. 9. There we show the dependence of σ_{Zh} and σ_{Ah} on M_A in the no-mixing scenario for $\tan\beta = 5$ and $\tan\beta = 50$. For σ_{Zh} , the A boson decouples quickly; the dependence on M_A becomes very weak for $M_A \gtrsim 250$ GeV, when σ_{Zh} is already practically constant (compare e.g. [13]). In the same limit, σ_{Ah} goes quickly to zero due to suppression of

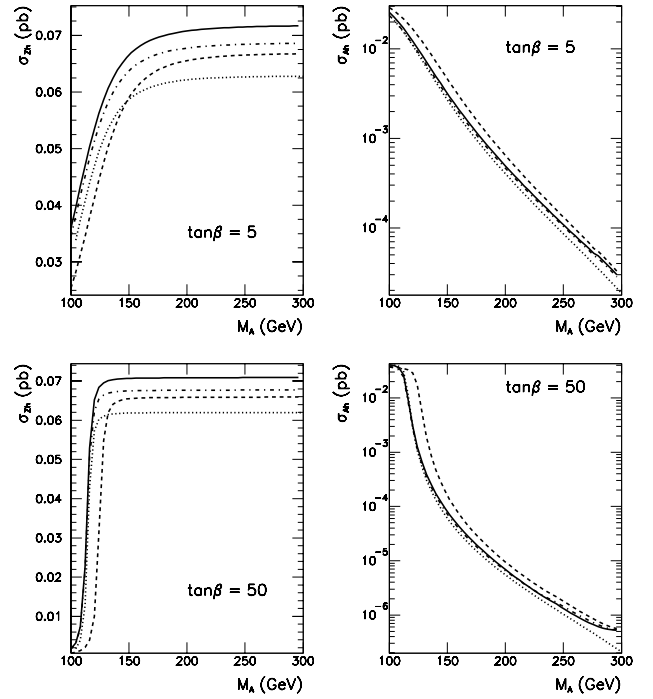


Fig. 9. σ_{Zh} and σ_{Ah} as a function of M_A at $\sqrt{s} = 500$ GeV, shown for $\tan\beta = 5$ and $\tan\beta = 50$, $X_t = 0$, and the parameters of Table 1. The solid (dot-dashed) line represents the two-loop FD result including (excluding) box contributions, the dotted line shows the RG α_{eff} approximation and the dashed line shows the one-loop FD result

the effective ZhA coupling, which is $\sim \cos(\alpha_{\text{eff}} - \beta)$; also the kinematical suppression plays a role, but this becomes significant only for sufficiently large M_A , $M_A > 350$ GeV. For large $\tan\beta$ the decoupling of M_A is even more rapid. The differences between the FD two-loop result and the RG α_{eff} approximation for the Higgs-strahlung cross section tend also to a constant, but they increase with M_A for the associated production. The latter can be explained by the growing relative importance of 3- and 4-point vertex function contributions compared to the strongly suppressed Born-like diagrams. As can be seen from Fig. 9, for $\tan\beta = 50$ and $M_A \geq 300$ GeV the FD two-loop result is almost an order of magnitude larger than the result of the RG α_{eff} approximation, and starts to saturate. This can be attributed to the fact that the (non-decoupling) vertex and box contributions begin to dominate the cross section value. However, such a situation occurs only for very small σ_{Ah} values, $\sigma_{Ah} \approx 10^{-3}$ fb, below the expected experimental LC sensitivities.

4 Conclusions

Using the Feynman-diagrammatic approach we have calculated the production cross sections for $e^+e^- \rightarrow hZ, hA$. The Higgs-boson propagator corrections have been evaluated, including besides the full one-loop result also the dominant and subdominant two-loop corrections. In addi-

tion we have included also the full set of one-loop vertex and box corrections.

We have also investigated an improved Born approximation based on the effective mixing angle, α_{eff} , in the neutral \mathcal{CP} -even Higgs sector. We have shown analytically that this approximation corresponds to taking into account the Higgs-boson propagator corrections with neglected external momentum at one-loop and two-loop order.

While the previous results available in the literature neglected the large two-loop corrections in the case of the Feynman-diagrammatic approach and were restricted to an improved Born approximation in the case of the renormalization-group improved one-loop Effective Potential approach, our new result combines the dominant two-loop corrections with the complete Feynman-diagrammatic one-loop result and thus represents the presently most precise prediction for the production cross sections for $e^+e^- \rightarrow hZ, hA$.

Specifically we have numerically analyzed the effect of the two-loop contributions incorporated in our result, which turned out to be sizable. We have furthermore compared our full Feynman-diagrammatic results for σ_{Zh} and σ_{Ah} with the approximation where α_{eff} and M_h are evaluated within the renormalization-group improved one-loop Effective Potential approach (RG α_{eff} approximation). For LEP2 energies, $\sqrt{s} = 206 \text{ GeV}$, the difference between the Feynman-diagrammatic result and the RG α_{eff} approximation stays mostly at the per cent level in the parameter space allowed by the LEP2 exclusion limits for M_h . At energies reachable at an e^+e^- linear collider, e.g. $\sqrt{s} = 500 \text{ GeV}$, the difference between the Feynman-diagrammatic result and the RG α_{eff} approximation can reach 10-15% for σ_{Zh} or even 25% for σ_{Ah} . The box contributions play an important role for high \sqrt{s} and can amount up to 10%. Therefore in a precision analysis for a high energy e^+e^- collider the two-loop propagator corrections as well as the complete diagrammatic one-loop contributions should be included⁶.

Acknowledgements. Parts of the calculation have been performed on the QCM cluster at the University of Karlsruhe, supported by the Deutsche Forschungsgemeinschaft (Forschergruppe ‘‘Quantenfeldtheorie und Computeralgebra’’) and by the European Union under contract HPRN-CT-2000-000149. This work has been supported in part by the Foundation for Polish-German Collaboration grant number 3310/97/LN and by the Polish Committee of Scientific Research under the grant number 2 P03B 052 16, 1999-2000 (S.H. and J.R.). We express our gratitude to K. Desch, P. Janot and A. Quadt for helpful discussions.

⁶ A public Fortran code for the production cross sections is in preparation [26].

Appendix Explicit expressions for the cross sections

Performing the sum over polarization states in (23) one gets for the associated scalar and pseudoscalar production:

$$\begin{aligned} \mathcal{A}_{1PS}^i &= -\mathcal{A}_{2PS}^i \\ &= \frac{e^2}{8} \lambda^2 (s, M_A^2, M_{H_i}^2) \left(|a_{PS}^i|^2 + |b_{PS}^i|^2 \right), \end{aligned} \quad (\text{A.1})$$

where

$$\begin{aligned} a_{PS}^i &= \hat{c}_V \left(2\tilde{V}_{ZPS}^{(0)i1} + \tilde{F}_P^{i1} + \tilde{F}_S^{i1} \right) \\ &\quad - 2\tilde{V}_{ZPS}^{(0)i1} \frac{\hat{\Sigma}_{\gamma Z}^T(s)}{D_\gamma(s)} + \left(\tilde{G}_P^{i1} + \tilde{G}_S^{i1} \right) \frac{D_Z(s)}{D_\gamma(s)}, \\ b_{PS}^i &= \hat{c}_A \left(2\tilde{V}_{ZPS}^{(0)i1} + \tilde{F}_P^{i1} + \tilde{F}_S^{i1} \right), \end{aligned} \quad (\text{A.2})$$

and λ as given in (22). The corresponding expressions for the Higgs-strahlung process are more complicated:

$$\begin{aligned} \mathcal{A}_{2ZS}^i &= -\frac{e^2 \lambda^2 (s, M_Z^2, M_{H_i}^2)}{32M_Z^2} \\ &\quad \times \left[|2a_{ZS}^i - (s + M_Z^2 - M_{H_i}^2) b_{ZS}^i|^2 \right. \\ &\quad \left. - 4sM_Z^2 |b_{ZS}^i|^2 + |2c_{ZS}^i - (s + M_Z^2 - M_{H_i}^2) d_{ZS}^i|^2 \right. \\ &\quad \left. - 4sM_Z^2 |d_{ZS}^i|^2 \right], \end{aligned} \quad (\text{A.3})$$

$$\mathcal{A}_{1ZS}^i = e^2 s \left(|a_{ZS}^i|^2 + |c_{ZS}^i|^2 \right) - \mathcal{A}_{2ZS}^i, \quad (\text{A.4})$$

where

$$\begin{aligned} a_{ZS}^i &= \hat{c}_V \left(\tilde{V}_{ZZS}^{(0)i} + \tilde{F}_1^i \right) - \tilde{V}_{ZZS}^{(0)i} \frac{\hat{\Sigma}_{\gamma Z}^T(s)}{D_\gamma(s)} + \tilde{G}_1^i \frac{D_Z(s)}{D_\gamma(s)}, \\ b_{ZS}^i &= \hat{c}_V \left(\tilde{F}_3^i - \tilde{F}_4^i \right) + \left(\tilde{G}_3^i - \tilde{G}_4^i \right) \frac{D_Z(s)}{D_\gamma(s)}, \\ c_{ZS}^i &= \hat{c}_A \left(\tilde{V}_{ZZS}^{(0)i} + \tilde{F}_1^i \right), \\ d_{ZS}^i &= \hat{c}_A \left(\tilde{F}_3^i - \tilde{F}_4^i \right). \end{aligned} \quad (\text{A.5})$$

The quantities \tilde{F} and \tilde{G} denote effective Higgs-gauge-boson vertex form factors. They can be defined as follows. At the tree level the relevant Higgs-boson vertices read (the assignment of momenta is given in Sect. 2.4):

$$V_{ZZS}^{(0)\mu\nu i} = iV_{ZZS}^{(0)i} g^{\mu\nu}, \quad (\text{A.6})$$

$$V_{ZPS}^{(0)\mu ij} = V_{ZPS}^{(0)ij} (p - q)^\mu, \quad (\text{A.7})$$

where $V_{ZZS}^{(0)i}$ and $V_{ZPS}^{(0)ij}$ can be written in matrix form as (index j numerates CP-odd Higgs bosons: $A \equiv P_1$, $G \equiv P_2$):

$$V_{ZZS}^{(0)i} = \frac{eM_Z}{s_W c_W} \begin{pmatrix} \cos(\alpha - \beta) \\ -\sin(\alpha - \beta) \end{pmatrix}, \quad (\text{A.8})$$

$$V_{ZPS}^{(0)ij} = -\frac{e}{2s_W c_W} \begin{pmatrix} \sin(\alpha - \beta) & \cos(\alpha - \beta) \\ \cos(\alpha - \beta) & -\sin(\alpha - \beta) \end{pmatrix}. \quad (\text{A.9})$$

After including one-loop vertex corrections the renormalized vertices have the form:

$$V_{ZPS}^{\mu ij} = p^\mu \left(V_{ZPS}^{(0)ij} + \hat{F}_P^{ij} \right) - q^\mu \left(V_{ZPS}^{(0)ij} + \hat{F}_S^{ij} \right), \quad (\text{A.10})$$

$$V_{ZZS}^{\mu\nu i} = i \left[g^{\mu\nu} \left(V_{ZZS}^{(0)i} + \hat{F}_1^i \right) + p^\mu p^\nu \hat{F}_2^i + q^\mu q^\nu \hat{F}_3^i + p^\mu q^\nu \hat{F}_4^i + q^\mu p^\nu \hat{F}_5^i \right], \quad (\text{A.11})$$

where \hat{F}_a 's are the renormalized vertex form factors.

Next, we define the respective quantities with tilde which are obtained by inclusion of the one-loop corrections on the external lines. For instance, the complete vertices read (in the following: $i' = 3 - i, j' = 3 - j$):

$$\tilde{V}_{ZPS}^{ij} = \left(\mathcal{Z}_{S_i}^{\text{ext}} \mathcal{Z}_{P_j}^{\text{ext}} \right)^{1/2} \left(V_{ZPS}^{ij} + \mathcal{Z}_{S_i}^{\text{mix}} V_{ZPS}^{i'j} + \mathcal{Z}_{P_j}^{\text{mix}} V_{ZPS}^{ij'} + \mathcal{Z}_{S_i}^{\text{mix}} \mathcal{Z}_{P_j}^{\text{mix}} V_{ZPS}^{i'j'} \right), \quad (\text{A.12})$$

and

$$\tilde{V}_{ZZS}^i = \left(\mathcal{Z}_Z^{\text{ext}} \mathcal{Z}_{S_i}^{\text{ext}} \right)^{1/2} \left(V_{ZZS}^i + \mathcal{Z}_{S_i}^{\text{mix}} V_{ZZS}^{i'} \right), \quad (\text{A.13})$$

where

$$\mathcal{Z}_Z^{\text{ext}} = \text{Re} \left(1 + \frac{\partial}{\partial q^2} \hat{\Sigma}_Z^T(q^2) \Big|_{q^2=M_Z^2} \right)^{-1}. \quad (\text{A.14})$$

The vertices \tilde{V}_{ZPS} , \tilde{V}_{ZZS} can be decomposed into $\tilde{V}_{ZPS}^{(0)}$, \tilde{F}_P , \tilde{F}_S etc. (as in (A.10,A.11)) where e.g. $\tilde{F}_1^i = \left(\mathcal{Z}_{S_i}^{\text{ext}} \right)^{1/2} \left(F_1^i + \mathcal{Z}_{S_i}^{\text{mix}} F_1^{i'} \right)$ etc.

To include photon exchange in the s -channel one needs to know also the renormalized vertices $V_{\gamma PS}$ and $V_{\gamma ZS}$ (which vanish at the tree level):

$$V_{\gamma PS}^{\mu ij} = p^\mu \hat{G}_P^{ij} - q^\mu \hat{G}_S^{ij}, \quad (\text{A.15})$$

$$V_{\gamma ZS}^{\mu\nu i} = i \left[g^{\mu\nu} \hat{G}_1^i + p^\mu p^\nu \hat{G}_2^i + q^\mu q^\nu \hat{G}_3^i + p^\mu q^\nu \hat{G}_4^i + q^\mu p^\nu \hat{G}_5^i \right]. \quad (\text{A.16})$$

The vertices $\tilde{V}_{\gamma PS}$, $\tilde{V}_{\gamma ZS}$ are defined similarly as shown in (A.12, A.13).

The explicit expressions for the one-loop corrections to the vertices V_{ZPS} , V_{ZZS} , $V_{\gamma PS}$ and $V_{\gamma ZS}$ can be found in [16].

References

1. G. Kane, C. Kolda, J. Wells, Phys. Rev. Lett. **70** (1993) 2686, hep-ph/9210242; J. Espinosa, M. Quirós, Phys. Rev. Lett. **81** (1998) 516, hep-ph/9804235
2. P. Igo-Kemenes, talk given at the LEPC meeting, 3rd of November 2000; The ALEPH collaboration, Phys. Lett. **B 495** (2000) 1, hep-ex/0011045; The DELPHI collaboration, CERN-EP 2001-004, to appear in Phys. Lett. **B**; The L3 collaboration, Phys. Lett. **B 495** (2000) 18, hep-ex/0011043; The OPAL collaboration, to appear in Phys. Lett. **B**, hep-ex/0101014
3. R. Brinkmann et al. (editors), Conceptual Design of a 500 GeV e^+e^- Linear Collider with Integrated X-ray Laser Facility, DESY 97-048; see also: TESLA TDR, obtainable from www.desy.de/~lcnotes/tdr/
4. A. Djouadi, W. Kilian, M. Mühlleitner, P.M. Zerwas, Eur. Phys. Jour. **C 10** (1999) 45, hep-ph/9903229
5. H. Haber, R. Hempfling, Phys. Rev. Lett. **66** (1991) 1815; Y. Okada, M. Yamaguchi, T. Yanagida, Prog. Theor. Phys. **85** (1991) 1; J. Ellis, G. Ridolfi, F. Zwirner, Phys. Lett. **B 257** (1991) 83; Phys. Lett. **B 262** (1991) 477; R. Barbieri, M. Frigeni, Phys. Lett. **B 258** (1991) 395
6. M. Carena, J. Espinosa, M. Quirós, C. Wagner, Phys. Lett. **B 355** (1995) 209, hep-ph/9504316
7. M. Carena, M. Quirós, C. Wagner, Nucl. Phys. **B 461** (1996) 407, hep-ph/9508343
8. H. Haber, R. Hempfling, A. Hoang, Z. Phys. **C 75** (1997) 539, hep-ph/9609331
9. R. Hempfling, A. Hoang, Phys. Lett. **B 331** (1994) 99, hep-ph/9401219
10. R.-J. Zhang, Phys. Lett. **B 447** (1999) 89, hep-ph/9808299
11. J. Espinosa, R.-J. Zhang, JHEP **0003** (2000) 026, hep-ph/9912236; Nucl. Phys. **B 586** (2000) 3, hep-ph/0003246
12. S. Heinemeyer, W. Hollik, G. Weiglein, Phys. Rev. **D 58** (1998) 091701, hep-ph/9803277; Phys. Lett. **B 440** (1998) 296, hep-ph/9807423
13. S. Heinemeyer, W. Hollik, G. Weiglein, Eur. Phys. Jour. **C 9** (1999) 343, hep-ph/9812472
14. W. Kilian, M. Krämer, P.M. Zerwas, Phys. Lett. **B 373** (1996) 135, hep-ph/9512335
15. P.H. Chankowski, S. Pokorski, J. Rosiek, Phys. Lett. **B 274** (1992) 191; Phys. Lett. **B 286** (1992) 307
16. P.H. Chankowski, S. Pokorski, J. Rosiek, Nucl. Phys. **B 423** (1994) 437; Nucl. Phys. **B 423** (1994) 497
17. A. Dabelstein, Z. Phys. **C 67** (1995) 495, hep-ph/9409375
18. V. Driesen, W. Hollik, Z. Phys. **C 68** (1995), 485, hep-ph/9504335
19. V. Driesen, W. Hollik, J. Rosiek, Z. Phys. **C 71** (1996) 259, hep-ph/9512441
20. J. Gunion, H. Haber, G. Kane, S. Dawson, The Higgs Hunter's Guide, Addison-Wesley, 1990
21. A. Djouadi, J. Kalinowski, P.M. Zerwas, Z. Phys. **C 57** (1993) 569; S. Dittmaier, M. Krämer, Y. Liao, M. Spira, P.M. Zerwas, Phys. Lett. **B 441** (1998) 383, hep-ph/9808433; Phys. Lett. **B 478** (2000) 247, hep-ph/0002035; S. Dawson, L. Reina, Phys. Rev. **D 57** (1998) 5851, hep-ph/9712400; Phys. Rev. **D 59** (1999) 054012, hep-ph/9808443; Phys. Rev. **D 61** (2000) 013002, hep-ph/9906419
22. P. Janot, in Physics at LEP2, eds. G. Altarelli, T. Sjöstrand, F. Zwirner, CERN 96-01, Vol. 2, p. 309
23. P. Janot, A. Quadt, private communication
24. A. Pilaftsis, C.E.M. Wagner, Nucl. Phys. **B 553** (1999) 3, hep-ph/9902371
25. S. Heinemeyer, W. Hollik, G. Weiglein, Eur. Phys. Jour. **C 16** (2000) 139, hep-ph/0003022

26. The two-loop corrections are contained in *FeynHiggs* and *FeynHiggsFast*: S. Heinemeyer, W. Hollik, G. Weiglein, *Comp. Phys. Comm.* **124** 2000 76, hep-ph/9812320; hep-ph/0002213. A public Fortran code for the production cross sections is in preparation. All codes are accessible via www.feynhiggs.de
27. S. Heinemeyer, W. Hollik, G. Weiglein, *Phys. Lett.* **B 455** (1999) 179, hep-ph/9903404
28. S. Heinemeyer, W. Hollik, G. Weiglein, *JHEP* **0006** (2000) 009, hep-ph/9909540; hep-ph/9912263
29. M. Carena, S. Heinemeyer, C. Wagner, G. Weiglein, hep-ph/9912223
30. M. Carena, H. Haber, S. Heinemeyer, W. Hollik, C. Wagner, G. Weiglein, *Nucl. Phys.* **B 580** (2000) 29, hep-ph/0001002
31. S. Andringa et al., Searches for Higgs Bosons: Preliminary Combined Results using LEP Data Collected at Energies up to 209 GeV, ALEPH 2000-074 CONF 2000-051, DELPHI 2000-148 CONF 447, L3 Note 2600, OPAL Technical Note TN661; A. Dedes, S. Heinemeyer, P. Teixeira-Dias, G. Weiglein, *Jour. Phys.* **G 26** (2000) 582, hep-ph/9912249